Pergamon

NanoStructured Materials, Vol. 11, No. 8, pp. 1361–1377, 1999
Elsevier Science Ltd

0965-9773/99/$–see front matter

PII S0965-9773(00)00433-5

PROCESSING AND MICROSTRUCTURE OF NANO-Mo/Al_2O_3 COMPOSITES FROM MOCVD AND FLUIDIZED BED

Ching-Jang Lin, Chih-Chung Yang and Wen-Cheng J. Wei*
Institute of Materials Science and Engineering, National Taiwan University, Taipei, Taiwan 106, Republic of China

(Received May 10, 1999)
(Accepted July 8, 1999)

Abstract—The process utilizing metal-organic chemical vapor deposition (MOCVD) was conducted in a fluidized Al_2O_3 powder bed for the preparation of nano-Mo ceramic composites. During the process, Mo species were deposited in fine Al_2O_3 ceramic powder using a pyrolysis of Mo carbonyl. The composition and crystallinity of the intermediate phases of $Mo_2C_xO_y$, and the microstructure of the coated particles and coated layer were analyzed using XRD/SEM/TEM techniques. The granulated powder was then treated by H_2 reduction, pressureless sintering or hot-pressing in a vacuum, which could achieve densities better than 99% T.D. The densification, wear, and microstructural properties of the dense nano Mo-composites were then investigated and discussed. It is seen that the nano-inclusion of Mo grains inhibited the grain growth of the alumina matrix, which had a mean grain size of either 4.9 μm or 1.2 μm, as the volume fraction of Mo increased from 0 vol% to 5 vol%. The wear resistance of the nano-Mo/Al_2O_3 was approximately 2 times better than that of pure Al_2O_3. Through an understanding of the pyrolysis of $Mo(CO)_6$ and grain growth kinetics of Mo-species growth kinetics, the morphology and size of the Mo grains in ceramic composites can be modified. *©2000 Acta Metallurgica Inc.*

Introduction

Several breakthroughs have been made in the past decade in high performance ceramics that possess properties capable of changing the traditional image of ceramic materials. The successful preparation of nano-size composites (1,2) may be the one of the strongest impacts on the ceramic community.

Nanocomposite materials are defined as composites of more than one Gibbsian solid phase where at least one of the phases shows dimensions in the nanometric range (1). Composites with nano-powder are reported to be good in mechanical properties and in reliability with the help of microstructural modification with reduced inherent flow size (3,4). In comparison, the classical ceramic processing routes using ultrafine (<50 nm) ceramic powder may hold certain disadvantages (5). Strong agglomeration and poor dispersion problems, for example, are two major concerns in colloidal processing (5,6).

Metallic particulates used as the reinforced phase have innate properties, such as plastic and electric conductivity. Transition metals, such as Ni, Cr, Mo, W melt at high temperature and have a high elastic modulus. However, the thermal expansion coefficient (TEC) of these metals show a wide range, from $4.59*10^{-6}$/°C (for W), or $5.43*10^{-6}$/°C (for Mo), to a fairly high value of $19.2*10^{-6}$/°C (for Ag) (7). The mismatch between the metallic inclusion and ceramic matrix generates various types of reinforcement. When considering electrical conductivity, TEC mismatches, melting points, and Young's modulus, the optimized choice of the metallic phase for making structural ceramic composite is W or Mo.

* Corresponding author: 1 Roosevelt Rd., Section 4, Taipei, Taiwan, 106, R.O.C.

Mo reinforced ceramic composites have been studied by several researchers (8–11). Recently, Nawa *et al*. (8,9) conducted a ball-milling process using acetone as the solution to prepare fine Mo/Al_2O_3 and W/Al_2O_3 mixtures. The fracture strength and toughness of the hot-pressed composites are significantly improved. In addition to wet-processing methods, a gas reaction technique can be utilized to synthesize nano-sized powder mixtures, a technique, which enables the growth of nanometric particles to start from a molecular-scale phase.

Chemical vapor deposition (CVD) and fluidized powder bed processes are two mature and commercial techniques widely used in the semiconductor and chemical engineering industries. McCreary (12) first reported the combination of processes used to deposit high atomic number metals (such as Ni, Mo, and Re) on micro-spherical glass in fluidized beds. The sources of the metallic phase were obtained from the pyrolysis of metal carbonyls at a reduced atmosphere.

MOCVD is one of the gas reaction processes. Wei and Lo (13,14) have extensively reviewed the process and properties of the (Mo, Cr) oxycarbides on various substrates, e.g. stainless steel and SiC, prepared using the metal-organic CVD (MOCVD) process. There were several concerns, however, about the processing conditions, including low deposition pressure, ultrafine particle size and agglomeration during deposition, etc. If the MOCVD process can be conducted in a fluidized powder reactor, it can potentially lead to nanometric dispersoid and homogeneous coating on submicron ceramic powders (15).

Wear properties among all the mechanical properties of nano-sized ceramic composites reported in literature (16–19) showed the most consistent results. The pinning of grain boundaries by these secondary inclusions resulted in a smaller grain size and wavy grain boundaries. The matrix grains are interlocking, therefore, the microstructure displays better performance in the wear resistance of the nano-SiC/Al_2O_3.

Modulus mismatch causing a change in the fracture mode in ceramic composites may also be responsible for the improvement in toughness of some nanocomposites. Huang and Lin (20) studied WC/Si_3N_4 ceramic composites and the role of elastic property mismatch in the failure of ceramic composites. The fracture may involve various mechanisms of crack-branching, crack-deviation, and/or crack-arrest, but the strength of composites increased when the initial crack was subcritically extended and arrested at the interface of the matrix. Strengthening and toughening are evident with the secondary metallic phase.

The objectives of the present study are several. The fabrication of the nano-Mo/Al_2O_3 composite by a new process—conducting MOCVD in a fluidized powder reactor—is the primary objective. Special emphasis is placed on the pyrolysis sequence of $Mo(CO)_6$ and the growth mechanisms of Mo-species in the H_2 reduction stage. Secondly, the densification and characterization of the composite are also conducted. The distribution of Mo inclusions may resolve the homogeneity and the interaction of the metallic grains with matrix Al_2O_3. As a consequence, the mechanical properties, e.g. wear resistance, could be improved. Finally, the relationship between microstructure and wear property of the nanocomposite is studied and discussed.

2. Experimental

2.1 Processing Operation

The fluidized powder reactor and an MOCVD system are constructed based on the schematic diagram shown in Fig. 1. Molybdenum hexacarbonyls ($Mo(CO)_6$, Alfa Chemicals Co., MA, USA) were placed in a source chamber and carried by N_2 gas (99.9% pure) at a flow rate of 0.5 to 2.0 l/min. Deposition of Mo-carboxyl was conducted in a fluidized alumina powder bed with a hot-wall reactor. The carbonyl

1. N_2 gas source
2. flowmeter
3. Mo(CO)6 source chamber
4. fluidized powder bed (reaction chamber)
5. pressure gauge
6. cold trap system
7. mechanical pump
8. thermal couple
9. temperature controller

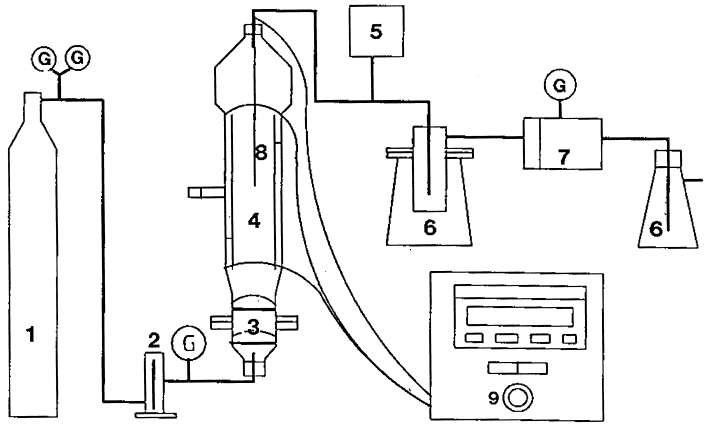

Figure 1. Schematic diagram of the MOCVD and fluidized powder bed equipment used in this research.

vapor flowed through the bottom of the fluidized powder bed and deposited on the fluidizing alumina powder (AKP-50, Sumitomo Chemical Co., Japan) which was preheated in a dry oven at 105°C and left overnight. Two gas outlets were attached to the top of the reactor, one for the measurement of absolute-pressure using a gauge with a variable capacitance sensor (MKS-Baratron, type 122A), the other, for vacuuming using a rotary pump installed with a cold trap system in front of the connection.

According to Lander's results (21), molybdenum carbonyl [$Mo(CO)_6$] evaporates readily in a vacuum system with a saturation pressure *P:*

$$\log P^* = 11.795 - 3800/T,$$

where T is the reaction temperature in Kelvin. The saturation pressure *P* of the carbonyl is 10.7 torr at 80°C. The source chamber was maintained at the pressure and kept at a constant 80°C in a water bath. When the temperature of the reactor was reached, a gas pressure of 10 torr was maintained through the whole coating stage. The coating temperature in the reactor was kept either at 250°C, 325°C or 400°C, and at a constant flow rate of N_2 in 2.0 l/min. The process was normally conducted for 2 hr or lasted for 1 to 4 hr when the coating temperature 325°C was selected.

In order to avoid the uncertainty of powder fluidization, the minimum fluidization velocity (U_{mf}) had to be determined (22–26). The flow rate was adjusted and controlled at 2000 ml/min of which was larger than the U_{mf} (ca. 736 ml/min) in this MOCVD process. Larger agglomerates (>20 μm) or heavy particles (coated with high density Mo-species) required greater floating forces which could be supplied by a greater flow rate. The deposited powder and a pure AKP-50 alumina (Sumitomo Chemical Co., LTD., Japan) were either pressureless sintered at 1600°C for 1 hr in H_2/Ar atmosphere (Tungsten-mesh furnace, Centorr Co., USA) or hot-pressed at 1400°C for 1hr in a vacuum. (High-Multi 5000 HP furnace, Fujidempa Kogyo Co., Ltd., Japan).

2.2 Characterization of Nanocomposites

The density variation of molybdenum oxycarbide deposited powder was measured using a pycnometer (Ultrapycnometer 1000, Quantachrome Co., USA). The thermogravimetric analyzer (TGA, Thermal Analyst 2000, DuPont Co., USA) was used to analyze the pyrolysis behavior of the composite powder processed at the temperature of either 250°C, 325°C or 400°C. The heating rate was 10°C/min tested in a constant flow of 5% H_2/N_2 atmosphere.

Crystalline phases of the deposited powder were identified with an X-ray diffractometer (XRD, PW1729, Philips Co., Holland). The morphology of deposited powder, the microstructure and composition of the sintered bulk were analyzed by a TEM (100CXII, JEOL Co., Japan) or an SEM (XL30, Philips Co., Holland) equipped with an X-ray energy dispersive spectroscopy (EDS, DX-4, EDAX Co., USA).

In this study, the wear resistance of pure alumina (AKP-50) and Mo/alumina was investigated using a wear tester (Multi-Purpose Friction and Wear Tester, TE53/7891, Plint & Partners Ltd., England). The test was performed under dry conditions, against an 800-mesh diamond wheel with a constant load of 42 N and under a constant rate of 200 rpm (equivalent to 0.1 m/s).

3. Result and Discussion

3.1 Density Variation

The density of the composite powder measured by pycnometer increases from 3.986 g/cm^3 of pure alumina powder to 4.033 g/cm^3 of the deposited powder. The deposited powder was tested by the semi-quantitative analysis of SEM-EDS which revealed 8 wt% of molybdenum species in the alumina powder. The density and EDS results of the composite powder show that Mo species have been incorporated in the alumina powder.

The density of pressureless sintered Mo/Al_2O_3 block (MA3-1) is 3.59 g/cm^3. Under the same sintering conditions, a pure alumina sample (AKP-50) shows a sintered density of 3.934 g/cm^3, which is equal to a 98.7% theoretical density (T.D.). The density of the hot-pressed composite block is 4.05 g/cm^3 (MA3-2/HP) and the open porosity is less than 0.02 vol%.

3.2 Pyrolysis of Molybdenum Carbonyl

Lander (21) first reported the use of metal carbonyls as the sources for metallic coatings. The vapor of Mo carbonyl was thermally pyrolyzed, then deposited on a substrate to form metal-related phases. In the early reports (27,28), the deposited film was characterized as a metal phase. However, minor contents of carbon or oxygen in the films found by those researchers were treated as impurities. The crystal structure of the 'Mo metal' phase of the coatings was indexed to be a face-centered cubic (FCC) structure, not the body-centered cubic (bcc) structure of molybdenum at room temperature. Recently, Ferguson *et al.* (29) have pointed out that the structure of the deposited phase is similar to Mo_2C with the chemical composition falling between $Mo_2C_{0.7}O_{0.6}$ and $Mo_2C_{0.6}O_{0.5}$. In addition, Wei and Lo (14) have studied the properties of the (Mo, Cr) oxycarbides under a similar MOCVD process. They reported that the coating phase of molybdenum carbonyl is $Mo_2C_xO_y$, structurally similar to Mo_2C, but the composition and crystalline structure may vary with deposition conditions (temperature and pressure).

McCreary (12) reported that molybdenum carbonyl sublimated at 315K and pyrolysized to Mo metal and CO gas at 623K. The given pyrolysis sequence is oversimplified due to the lack of knowledge of the effects of deposition temperature. Three TGA curves of the composite powders obtained either at

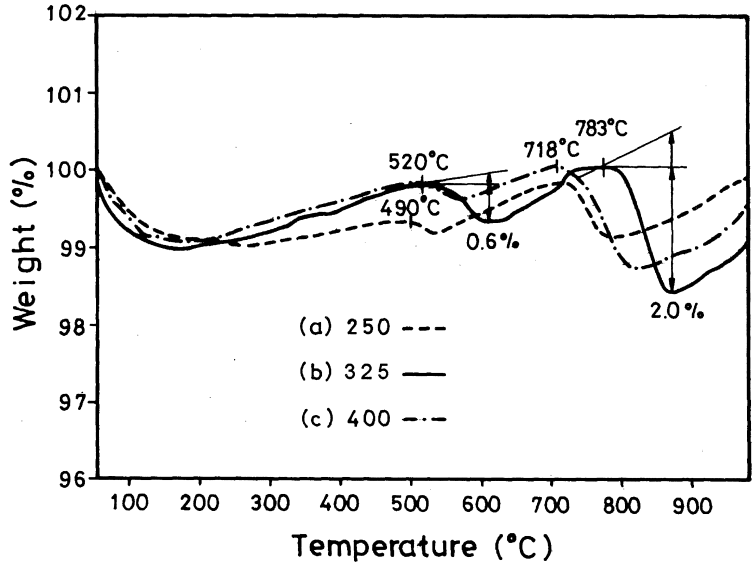

Figure 2. TGA results of $Mo_2C_xO_y/Al_2O_3$ powders obtained at various deposited temperatures (a) 250°C, (b) 325°C, and (c) 400°C. The testing condition is 10°C/min in 5% H_2/N_2 atmosphere.

250°C, 325°C or 400°C are shown in Fig. 2. Each curve has two stages of weight loss. The drifting of the curves, which occurred from 50 to 100°C, is due to the shift of the base-line to the equilibrium condition of the TGA instrument. The first weight loss happens from 490 to 618°C and the second weight loss occurs between 718 to 883°C as tested in 5%H_2/N_2 atmosphere. The first and second stages of weight loss, either 0.6 wt% or 2.0 wt%, are caused by the reduction of Mo-species. The reduction is first transformed to MoO_2, then to the Mo phase.

In order to confirm the TGA results, we selected 650°C and 900°C as the temperatures of the heat treatment. The composite powders in different stages of the heat treatment were analyzed by XRD. Fig. 3 displays the XRD results of a 5 vol% Mo/Al_2O_3 deposited powder at the temperatures in an H_2/N_2 atmosphere. The spectra show that the 325°C as-deposited phase is an amorphous molybdenum oxycarbide, resulting in the broadening of the XRD peak from 22° to 30° (2 θ angle). With the treatment at a higher temperature, the amorphous phase in deposited powder decomposes and forms the MoO_2 crystalline phase at 650°C treated for 1hr, and further reduces to Mo metal at 900°C for 1hr in 10%H_2/N_2 atmosphere.

The pyrolysis occurs through the breakage of Mo-(CO) bonds in the fluidizing powder bed reactor, and can be shown as the following sequential reactions:

80°C in 10 torr

$$Mo(CO)_{6(s)} \rightarrow Mo(CO)_{x(g)} + (CO)_{6-x(g)} \quad (1)$$

50°C to 400°C in flowing N_2

$$Mo(CO)_{x(g)} \rightarrow Mo_2C_xO_{y\,(s)}\ (\text{amorphous}) \quad (2)$$

490°C to 620°C in 10%H_2/N_2

$$Mo_2C_xO_{y\,(s)} \rightarrow MoO_{2(s)}\ (\text{crystalline}) + H_2O_{(g)} + CO_{2(g)} \quad (3)$$

650°C to 900°C in 10%H_2/N_2

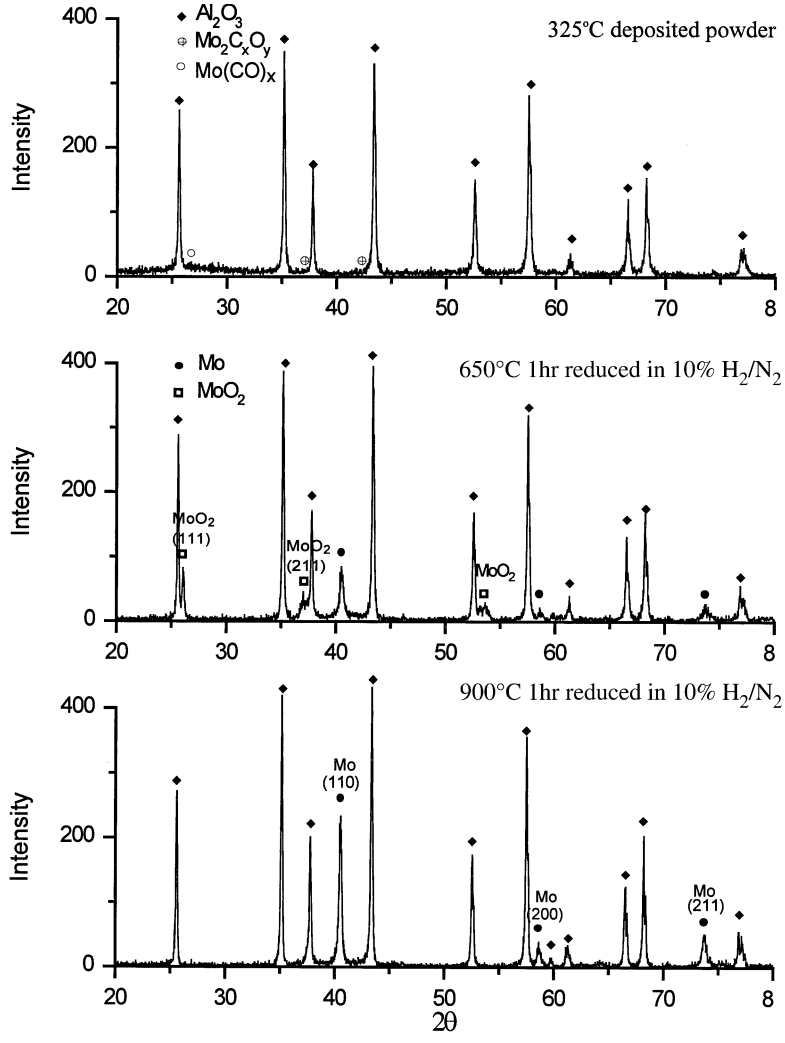

Figure 3. XRD results of 5 vol% Mo/Al_2O_3 composite powders deposited at various reduced temperatures.

$$MoO_{2(s)} \rightarrow Mo_{(s)}\ (\text{crystalline}) + H_2O_{(g)} \quad (4)$$

3.3 Microstructure and Microstructural Development

3.3.1 Deposited Particles and Sintered Block. TEM morphology of several Mo-species/Al_2O_3 particles prepared from the MOCVD in the fluidized powder bed is shown in Fig. 4. The coating features can be divided into two types, either smooth coating 'S' or granular deposits 'G'. The features of the granular surface are irregular with darker spots of sizes ranging from 6 nm to 30 nm. In addition, certain area is covered with a smooth amorphous film of Mo-species on Al_2O_3 particles. These features as indicated with 'S' markers (in Fig. 4) show the atomic adsorption effect on the electron beam. The contrast in the coating region changes gradually.

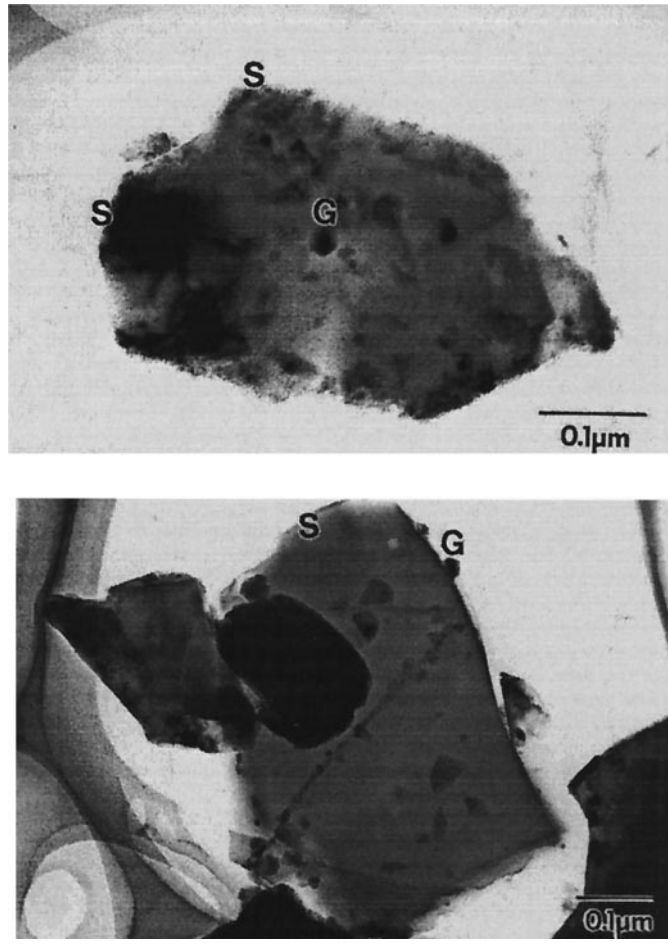

Figure 4. TEM micrographs of the composite particles.

The SEM morphologies of one pressureless sintering composite are shown in Fig. 5(a). The homogeneity of the sintered Mo/Al_2O_3 nanocomposite is in the scale of 50–150 μm (Fig. 5(a)) and the composition of the brighter (marker "b") and darker area (marker "d") contain 15 wt% or 5 wt% of Mo which was quantified by the EDS. The correspondent EDS pattern of bright ("b") regions is shown in Fig. 5(b). The inhomogeneity of pressureless sintered sample is a matter of agglomerate formation caused by non-uniformity in the fluidizing bed. However, the inhomogeneous structure will be prevented when hot-pressing is utilized. Fig. 6 shows the polished surfaces of hot-pressed composites, which use the same batch of composite powder as in Fig. 5(a). The agglomeration features in the scale of 200 μm are hardly observed, as shown in Fig. 6. Instead, submicron Mo features in bright contrast are still evident. Hot pressing and the atmosphere (vacuum) play an important role in the homogenization of the texture. During the previous coating process, only the minimal segregation of Mo and maximal homogeneity in hot-pressed composites were obtained when the agglomeration and second-phase additives were well dispersed in composite powder.

A series of TEM micrographs of three dense Mo/Al_2O_3 composites are shown in Fig. 7 illustrating Al_2O_3 composites with various types of Mo distribution. Fig. 7(a) shows the MA3-2 sample, which was pressureless-sintered at 1600°C for 1 hr in an H_2/Ar atmosphere and consisted of 5 vol% Mo in sizes

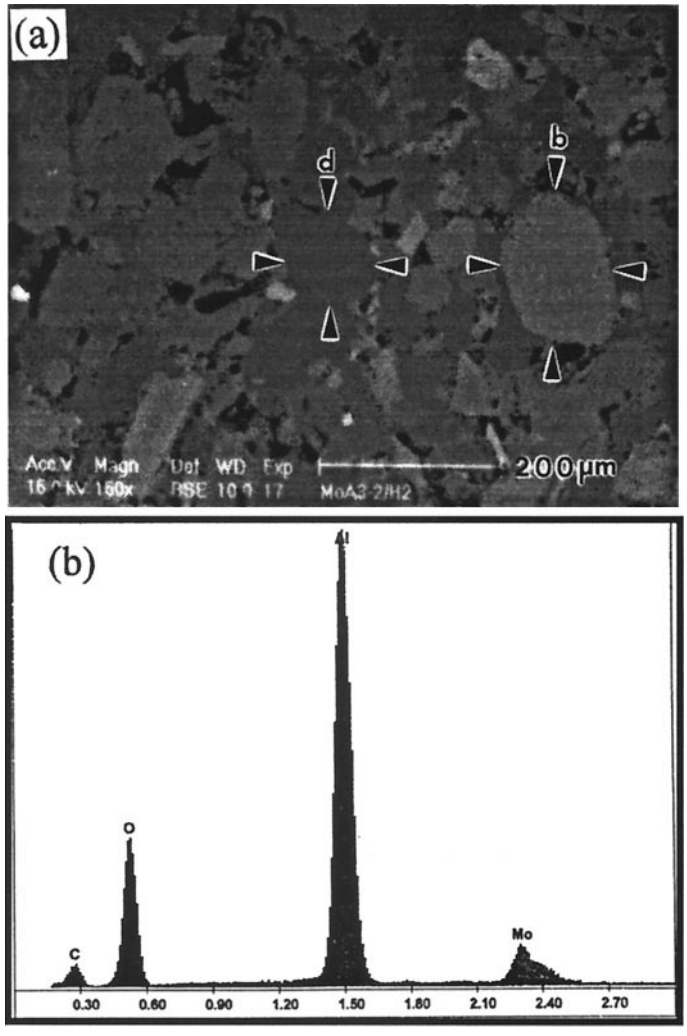

Figure 5. (a) SEM micrograph of 15 wt% Mo/Al_2O_3 nanocomposite imaged by back scattered (BS) mode; (b) EDS pattern of the "b" region pointed in the micrograph. The sample was pressureless-sintering in H_2/Ar atmosphere

of 50 to 200 nm. Most of the Mo grains are inter-granular, and the average grain size of Al_2O_3 is 1.2 μm in this MA3-2 composite.

The MA3-1 sample contained 2 vol% Mo grains in sizes of 5 to 50 nm sintered under the same conditions as in the previous sample (MA3-2), as shown in Fig. 7(b), revealing an average grain size of 0.8 μm Al_2O_3 matrix. Fig. 7(c) is the morphology of the MA3-2/HP sample, which contains 5 vol% Mo in sizes of 50 to 700 nm. The MA3-2/HP was hot-pressed at 1400°C for 1 hr in a vacuum atmosphere. The average grain size of the Al_2O_3 in Fig. 7(c) is 1.6 μm. The Mo phase with a large size distribution could be the result of the variation of crystallization behavior and grain growth at the sintering temperature.

A bright-field (BF) TEM micrograph of an Mo grain at the boundaries of Al_2O_3 grains is shown in Fig. 8. The corresponding diffraction pattern (DP) is indexed as the crystalline BCC phase of Mo. Clean interface between Mo/Al_2O_3 is evident. A higher content of Mo in Al_2O_3 matrix inhibits the grain

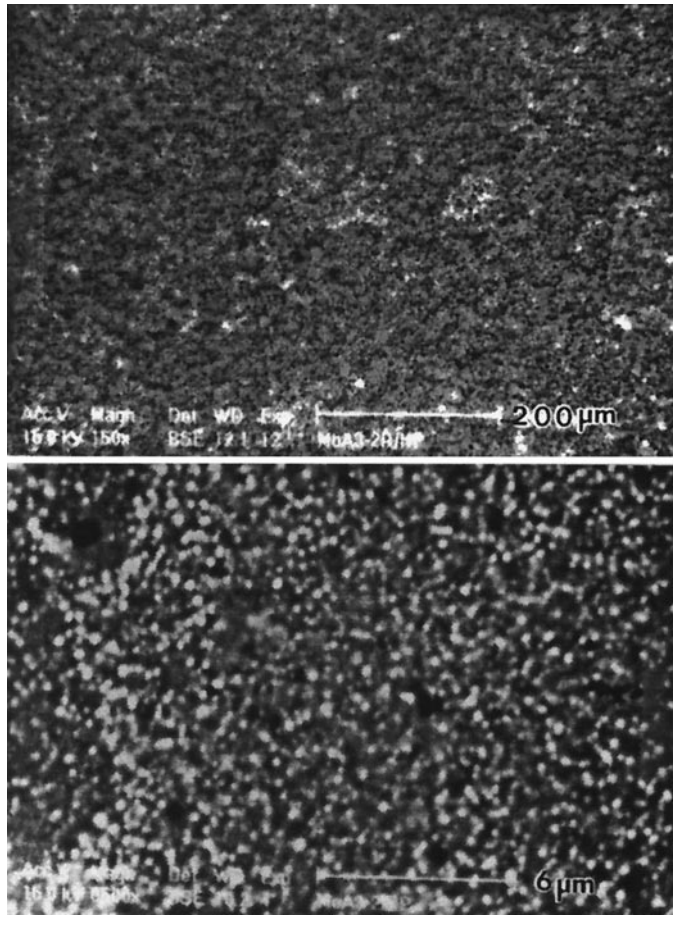

Figure 6. SEM micrographs in different magnifications imaged by back scattered (BS) mode. The composite was prepared by hot-pressing (HP) in vacuum atmosphere.

growth of Al_2O_3. In the opposite case, fewer (<5 vol%) and finer (<50 nm) Mo grains can not effectively inhibit the coarsening of Al_2O_3. These finer Mo grains are likely engulfed in Al_2O_3 grains as they grow. In this composite system, the mean grain size of Al_2O_3 matrix decreases to 1.2 μm as the volume fraction of second-phase Mo content increases to 5 vol% with pressureless sintering at 1600°C for 1 hr in H_2/Ar atmosphere.

3.3.2 Grain Growth Mechanism. The TEM studies on Mo/Al_2O_3 nanocomposites reveal that Mo grains belonging to inter- and/or intra-granular are controlled by pyrolysis reactions, the volume fraction of Mo, and the sintering atmosphere. The amorphous phase nucleated to form MoO_2 below 620°C, and further reduced to metal Mo at elevated temperatures. The crystallization and grain growth of Mo took place before the rearrangement of Al_2O_3 grain in the first stage of sintering. The grain growth of the Mo phase may be due to the transport of Mo-species by diffusion either along the surface or on the grain boundaries of the matrix.

The primary reason for the production of intra-type Mo is mainly induced by the grain growth of Al_2O_3 in sintering stage. The dragging force of these fine Mo (<200 nm) is not strong enough to pin the grain boundary of Al_2O_3 in position. As a result, the Mo is engulfed in the growing Al_2O_3. Under opposite conditions, large Mo grains stayed at Al_2O_3 grain boundaries throughout the entire sintering

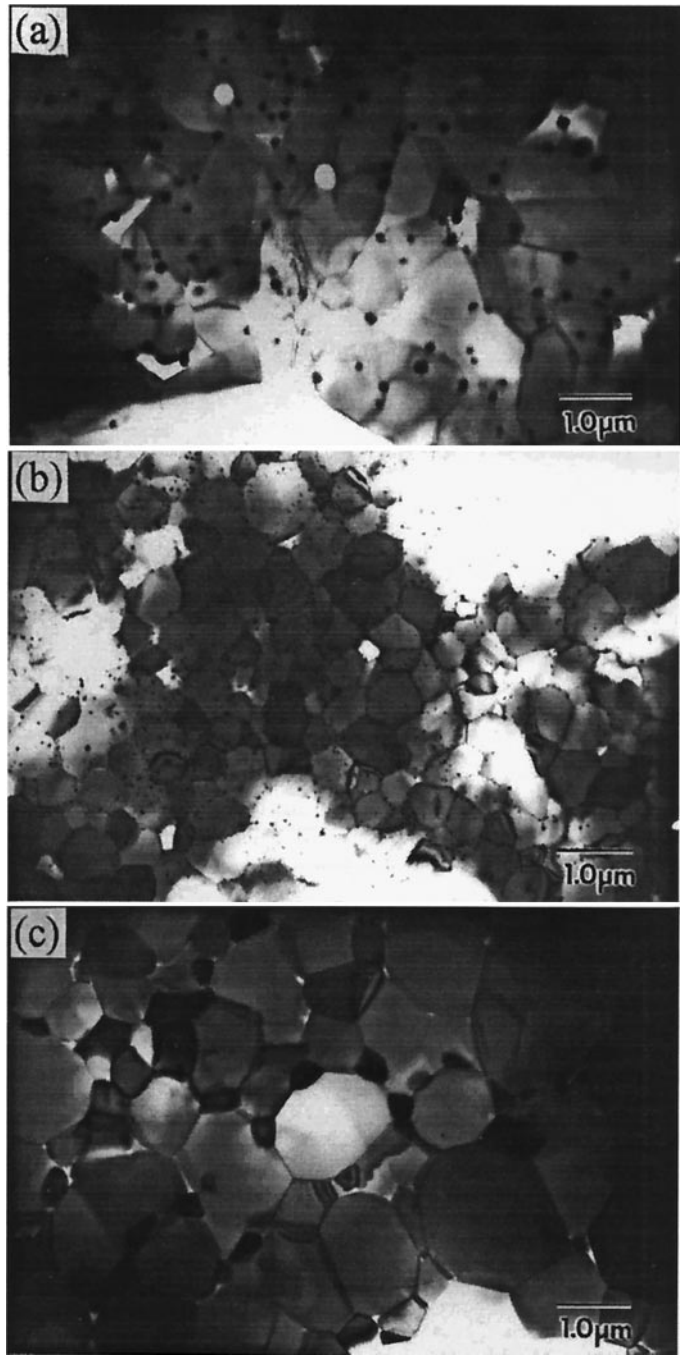

Figure 7. TEM micrographs of three sintered Mo/Al_2O_3 composites with (a) intergranular nano-sized Mo grains, (b) inter- and intra-Mo grains in the MA3-1 sample, and (c) inter-submicron and intra-nano-sized Mo grains in the MA3-2/HP sample

process, resulting in smaller Al_2O_3 grains. Previous results of the grain sizes could be interpreted with the *Zener relation* (30,31), $R_c = 4r/3V_f$, where r and Vf are the radius and the volume fraction of the

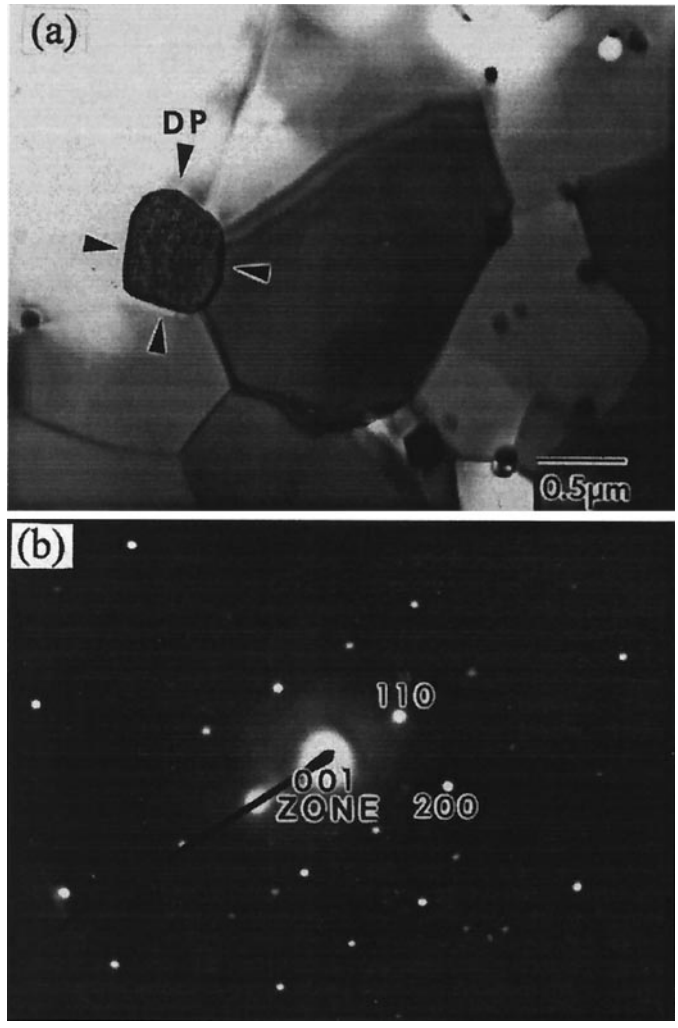

Figure 8. (a) Bright-field micrograph of Mo/Al_2O_3, and (b) diffraction pattern of the Mo as pointed "DP" in the micrograph.

second phase, respectively. This simple and approximate relationship shows that the critical size (*Rc*) of the matrix grains decreases as the particle size of effective inclusions decrease and the volume fraction increases.

The partial pressure of oxygen is still high enough to form MoO_2 and MoO_3 phases (32) at temperature below 1200°C when sintering under a rough vacuum condition. Sintering the composites containing Mo in an H_2 atmosphere can avoid the formation of the MoO_2 or MoO_3 phase. The melting point of Mo is 2610°C. The neck growth of Mo particles may occur at 1200°C. However, densification (or large shrinkage) of Mo particles is apparent at temperatures higher than 1600°C due to the low diffusion rate of Mo in the H_2/Ar atmosphere. The results depict that the microstructure of Mo/Al_2O_3 is controlled by the content of Mo and a sintering atmosphere.

From the results, it can be seen that the microstructure of the composite can be designed by adjusting or optimizing processing parameters, such as the content of Mo, the sintering atmosphere, temperature, pressure, and special arrangement of powder packing to fabricate at least five types of the Mo

TABLE 1
The Processing Conditions of Various Mo/Al_2O_3 Ceramic nanocomposites

Type	Range of Mo content	Atmosphere	Temperature and Pressure	Special Arrangement
inter-granular	5 to 15 vol%	H_2/Ar	Pressureless at 1600°C	well mixing
inter- and intra-granular	1 to 4 vol%	H_2/Ar	Pressureless at 1600°C	well mixing
inter-submicron and intra-nano-granular	5 to 15 vol%	vacuum	25 MPa HP at 1400°C	well mixing
inter-continuous and intra-nano-granular	>16 vol%	vacuum	25 MPa HP at 1400°C	well mixing
laminated layer and intra-nano-granular	Mo layer and <5 vol%	vacuum or H_2/Ar	Pressureless at 1600°C Or 25 MPa HP at 1400°C	layer stacking

metal/ceramic nanocomposite. The conditions that are optimal for the fabrication of different types of the nanocomposite are shown in Table 1. The features of microstructures of Mo grains in Al_2O_3 matrix could be (a) pure inter-granular, (b) inter- and intra-granular, (c) inter-submicron and intra-nano-granular, (d) inter-continuous and intra-nano-granular, or (e) laminated layer and intra-nano-granular Mo/Al_2O_3 nanocomposites. Three schematic diagrams are shown in Fig. 9 to reveal two-dimensional features of the metal/ceramic nanocomposites.

3.4 Wear Resistance

The relationship between Mo/Al_2O_3 composites and wear results of the samples is shown in Table 2 which lists the processing conditions of the samples, the sintered density, wear test parameters, and wear resistance results. The preliminary testing results showed that the diamond wheel should be dressed after every four thousand cycles in order to maintain good surface conditions. Therefore, the wear was tested under the conditions similar to those of the diamond wheel.

The wear results of pure alumina and Mo/Al_2O_3 are shown in Fig. 10. The wear rate of pure alumina is nearly two times greater than that of Mo/Al_2O_3 composites, either MA3-1 or MA3-2. It is believed that the addition of nano-sized molybdenum to aluminum oxide helps improve the wear resistance of pure alumina. First of all, a higher content of Mo in the Al_2O_3 matrix inhibits the grain growth of Al_2O_3. The refinement of the matrix grains can remarkably decrease the grain size and critical flow size, which probably enhance the mechanical properties of the surface layer (16).

The wear resistance of the MA3-2/HP is superior to pure Al_2O_3, but inferior to that of MA3-1 or 3-2. The sintering atmosphere of HP is a vacuum, but that of MA3-1 and 3-2 is H_2/Ar. The density of the HP sample is highest among those samples. On the other hand, the grain size of Mo and Al_2O_3, which is sintered in H_2/Ar, is finer than those sintered in a vacuum.

Fig. 11 shows the TEM micrographs of the Mo/Al_2O_3 nanocomposite. Figs.11(a) and 11(b) show second-phase Mo grains located at Al_2O_3 grain boundaries. Note that Mo grains are trapped at the boundaries and result in a wavy grain boundary. Similar observations have been reported by Harmer (19) and his colleague in the nano SiC/Al_2O_3 composite system. The matrix grains are interlocking, therefore, response for a better wear resistance to grain-pull-out during the test.

Fig. 11(c) shows the network of dislocations in the Al_2O_3 grain, perhaps resulting from the different thermal expansion coefficients between matrix (Al_2O_3: α 61 $7.8*10^{-6}$/°C) and second phase (Mo: $\alpha = 5.43*10^{-6}$/°C). Large internal stresses may be generated during cooling from the fabrication temper-

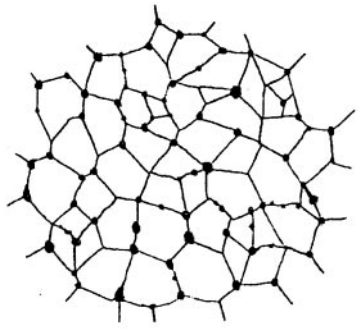

Inter-granular
metal/ceramic nanocomposite

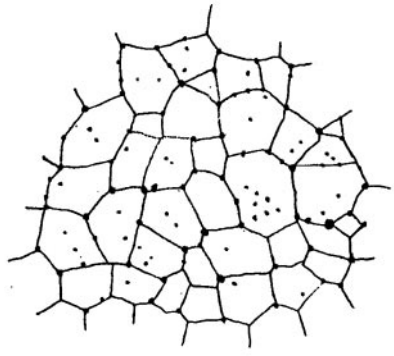

Inter- and intra-granular
metal/ceramic nanocomposite

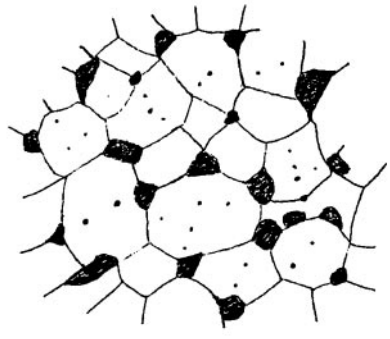

Inter-submicron and intra-nano-granular
metal/ceramic nanocomposite

Figure 9. Schematic classification of three Mo/Al_2O_3 nanocomposites.

ature 1400°C, e.g. hot-pressing. The results also imply the possibility of the occurrence of subgrains or a low angle grain boundary for strengthening the nanocomposites. As a result, wear resistance can significantly improve.

TABLE 2
The Fabrication Conditions, Wear Test Parameters and Wear Rate of Mo/Al_2O_3 Composites and Pure Al_2O_3

Sample	Deposition conditions	Sintering conditions	Bulk density (g/cm^3)	Wear rate (mm^3/Nm) After 10000 revolutions
A16-SG		1600°C/1 hr	3.92	5.47×10^{-4}
MA3-1	1 hour at 325°C	1600°C/1 hr	3.59	2.66×10^{-4}
MA3-2	2 hours at 325°C	1600°C/1 hr	3.31	2.52×10^{-4}
MA3-2/HP	2 hours at 325°C	1400°C/1 hr + HP	4.05	3.68×10^{-4}

Wear conditions: The applied load is 42 N corresponding to 1.0 ± 0.3% MPa and 200 rpm (0.1 m/s).

4. Conclusion

The objectives of this work are to develop a new synthesizing process and to fabricate different types of nano-Mo/Al_2O_3 composite through an understanding of the grain growth mechanism and the control of the microstructure. The results are summarized below.

1. The process utilizing metal-organic chemical vapor deposition (MOCVD) conducted in a fluidized powder bed can offer the opportunity to fabricate Mo/Al_2O_3 nano-composites with high density. The content of Mo can range from 1 to 15 vol% and the sizes of Mo grains ranging from 5 to 700 nm.

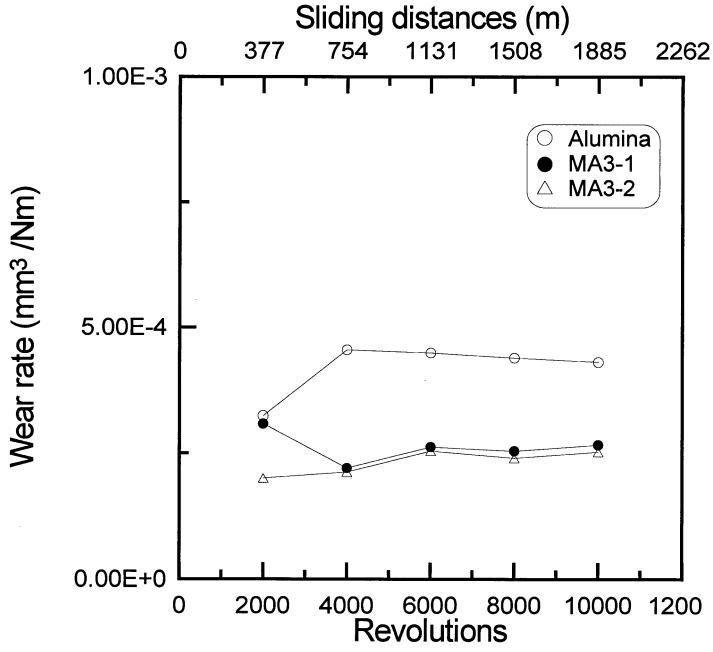

Figure 10. Wear results of Mo/Al_2O_3 nanocomposites and pure alumina.

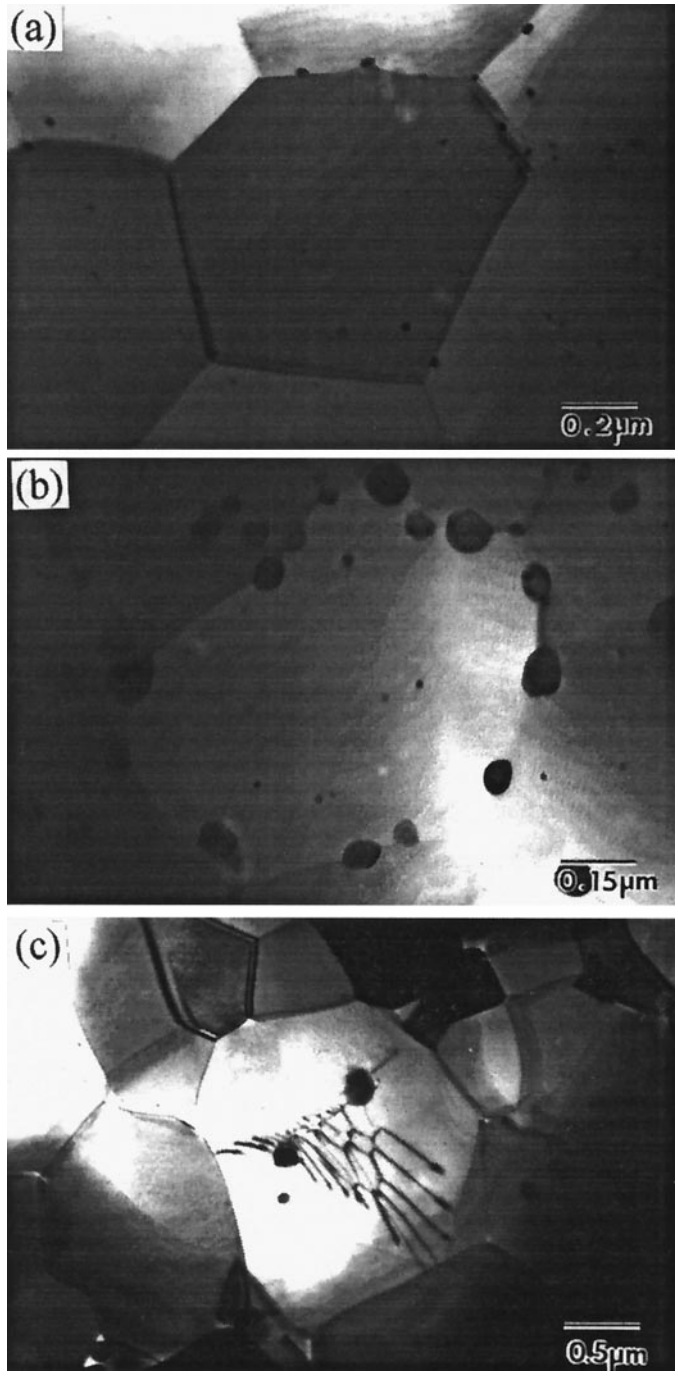

Figure 11. TEM micrographs of Mo/Al_2O_3 nanocomposites illustrating (a) nano-sized Mo inclusions at grain boundaries, (b) wavy grain boundaries pinning by Mo grains, and (c) the dislocation network associated with Mo inclusions in Al_2O_3 grain.

2. The constructed nano-Mo/Al_2O_3 composites show an average grain size of Al_2O_3 varying from 4.9 μm to 1.2 μm as the volume fraction of second-phase Mo increases from 0 vol% to 5 vol%.
3. The grain size of Mo sintered in H_2/Ar is finer than that sintered in a vacuum. The results may be due to the sintering in H_2/Ar which can avoid the formation of Mo oxides which have a higher diffusion rate or different diffusion routes than that of Mo.
4. A grain growth mechanism of Mo/Al_2O_3 nanocomposites is proposed. Mo diffusion through the surface and/or grain boundary takes place before the densification of matrix. However, the Mo grains tend to coalesce as soon as the Al_2O_3 grain grows in the matrix occurring in the final stage of sintering or hot pressing.
5. Various microstructures consisting of the Mo incorporated in the Al_2O_3 matrix can be made by varying the content of Mo, the sintering atmosphere, sintering temperature and the type of sintering.
6. It is believed that the addition of nano-sized Mo grains into Al_2O_3 matrix improves the wear resistance of pure alumina. The remarkable decrease in grain size and critical flow size is the factors of improvement. The second phase Mo grains act as a barrier to Al_2O_3 boundaries and form wavy grain boundaries.

Acknowledgment

The authors would like to acknowledge the research funding provided by the National Science Council (NSC) in Taiwan under contract NSC88-2216-E-002-028.

References

1. R. Roy, R.A. Roy, and D.M. Roy, Mater. Lett. 4, 323 (1986).
2. K. Niihara and A. Nakahira, J. Ceram. Soc. Jpn. pp. 404–417 (1991).
3. Y. Kinemuchi, T. Yanai, and K. Ishizaki, Nanostruct. Mater. 9, 23 (1996).
4. G. Pezzotti, V. Sergo, K. Ota, O. Sbaizero, N. Muraki, T. Nishida, and M. Sakai, J. Ceram. Soc. Jpn. 104, 479 (1996).
5. M. Sternitzke, J. Europ. Ceram. Soc. 17, 1061 (1997).
6. L.C. Stearns and M.P. Harmer, J. Am. Ceram. Soc. 79, 3013 (1996).
7. S.F. Wang, J.P. Dougherty, W. Huebner, and J.G. Pepin, J. Am. Ceram. Soc. 77, 3051 (1994).
8. M. Nawa, T. Sekino and K. Niihara, J. Mat. Sci., 29, 3185–3192 (1994).
9. M. Nawa, K. Yamazaki, T. Sekino, and K. Niihara, Mat. Letters 20, 299–304 (1994).
10. S.C. Wang and W.J. Wei, 1998, Nanostruct. Mater., Vol. 10, No. 6, pp. 983–1000 (1998).
11. W.J. Wei, S.C. Wang and F.H. Cheng, Nanostruct. Mater., Vol. 10, No. 6, pp. 965–981 (1998).
12. W.J. McCreary, "Microspherical laser targets by CVD," Proc. 5th Int. Conf. On CVD Electrochemical Society, Princeton, NJ, 714–725 (1975).
13. Ming-Hung Lo and Wen-Cheng J. Wei, J. Mater. Res., Vol. 11, No. 8, Aug 1996.
14. Wen-Cheng J. Wei and Ming-Hung Lo, Appl. Organometal. Chem., Vol. 12, 201–220 (1998).
15. H. Hahn, Nanostruct. Mat., Vol. 9, 3–12 (1997).
16. K. Niihara, J. Ceram. Soc. of Jap. vol. 99, 945–952, (1991).
17. T. Ohji, Y. K. Jeong, Y. H. Choa, and K. Niihara, J. Am. Ceram. Soc., 81[6] 1453–60 (1998).
18. R. W. Siegel, Nanostructured Mater., Vol. 4, No. 1, pp. 121–138 (1994).
19. A.M. Thompson, J. Fang, H.M. Chan, and M.P. Harmer, in *Ceramic Transaction Vol 51, Ceramic Processingand Science*, ed. H. Hausner, G.L. Messingand, S.I. Hirano, pp. 671–78, The Am. Ceram. Soc.
20. Jow-Lay Huang, Ching-Jang Lin, J. Mater. Sci., 28, 1074–80 (1993).
21. J.J. Landerand, L.H.Germer, *Platingmolybdenum, tungsten and chromium by thermal decomposition of their carbonyls*, Am. Inst. Metal. Eng. Tech. Pub. No. 2295, Sept. (1947).
22. D. Geldart, Powder Technol., 7, 285–290 (1973).
23. M. Kwauk, *Fluidization, idealized and bubbleless, with applications*, Chap. 14: Powder assessment, Ellis Horwood, NY, 229–232 (1992).
24. Nicholas P. Cheremisinoff and Paul N. Cheremisinoff, *Hydrodynamics of gas-solid fluidization*, Gulf Publishing Co. Londonetal. (1986).

25. S. Morooka, K. Kusakabe, A. Kobataand, Y. Kato, J. Chem. Eng. Jpn., 21, 41–46 (1988).
26. C.Y. Wen and, Y.H. Yu, A.I. Ch. E. Jour., 12, 610 (1966).
27. F. Okuyama and Y. Fujimoto, J. Appl. Phys. 56 566 (1984).
28. D.K. Flynn, J.I. Steinfeld and D.S. Sethi, J. Appl. Phys. 59 3914 (1986).
29. I.F. Ferguson, J.B. Hinseough, D. Morseand A.W. Miller, Nature (London) 202 1327 (1964).
30. Y.M. Chiang, D. Birnie III, and W.D. Kingery, *Physical Ceramics*, John Wiley & Sons, New York (1997).
31. R.J. Brook, J. Am. Ceram. Soc., 52, 59 (1969).
32. P. Gorden, *Principles of phase diagrams in materials systems*, McGraw-Hill, 1968.